Journal Article

Radiation Optimization for Phased Arrays of Antennas Incorporating the Constraints of Active Reflection Coefficients

Chou, H. -T., Wu, R. -Z., Akinsolu, M. O., Liu, Y. and Liu, B.

Recommended citation:

Radiation Optimization for Phased Arrays of Antennas Incorporating the Constraints of Active Reflection Coefficients

Hsi-Tseng Chou, *Fellow, IEEE*, Rui-Zhe Wu, Mobayode O. Akinsolu, *Senior Member, IEEE*, Yushi Liu, and Bo Liu, *Senior Member, IEEE*

Abstract—**High-power radiations from active antenna arrays may result in strong reflected power to cause RF device breakdown by the strong interelement mutual coupling. An excitation weighting synthesis of antenna arrays incorporating the constraint of active reflection/transmission coefficients between antenna elements is presented to optimize the radiation. It may enhance interelement isolation, reducing the effort of using sophisticated hardware-based structures that have difficulty in broad-angle beam steering. In the synthesis, the cost functions incorporate the difference between the optimized and the predefined excitation weightings of radiation patterns with limited reflected power or active reflection coefficients as a constraint. This article first introduces the basic concept to show the operational mechanisms. Practical definitions of cost functions are described to synthesize the radiation pattern considering the mutual coupling effects. The case without setting an initial desired radiation pattern is also examined for comparison. Numerical full-wave simulations are presented to validate the synthesis concepts by examining the characteristics of gain, sidelobe level (SLL), and port reflection coefficients.**

Index Terms—**Active pattern, antenna array, antenna coupling, array synthesis, differential evolution (DE), embedded pattern.**

I. Introduction

ACTIVE phased arrays of antennas are popularly used in radar and wireless communication systems to produce high antenna gains and beam-steering functionality for adequate wide-angle radio coverage. The high-power radiation may result in severe problems when the unavoidable electromagnetic (EM) mutual couplings between antenna elements are vital. In addition to the well-known behavior of impedance mismatches, causing scan blindness and signal cross-talks, the high reflected power in the transmitting modes may cause system breakdowns, particularly severe at wide-angle beam scans. In such cases, the radiation patterns may also cause gain losses, cross-polarization level (XPL) excess, and sidelobe levels (SLLs) degradation.

Active reflection coefficients (ARCs) were introduced [1], [2] for RF-device-fed arrays to justify such irregular behaviors and impacts on the system, where the active element pattern (AEP) concept was also introduced in [3] and further investigated by [4] and [5] to explore the radiation characteristics. AEP is the antenna element's radiation in the array environment with only its port excited with the others terminated, which is also referred to as the embedded element patterns (EEPs) [6], [7], [8], [9], [10], [11], [12], [13], [14] in the radiation pattern optimization. AEP incorporates the mutual coupling effects, in contrast to the standing-alone antenna's radiation [referred to as the isolated element pattern (IEP)]. The EEP provides an explicit expression to describe the AEPs' behaviors in the pattern optimization for the ARC improvement.

To suppress the array's ARC or reflected power, it is intuitive to reduce the interelement EM mutual couplings. Increasing the interelement's separation distance is most straightforward but will increase the array's physical size and raise the risk of producing grating lobes to limit the scan range. Orthogonal or diagonal placement of antenna distribution is another solution, which can create isolation larger than 15 dB [15], [16]. Still, this design takes a large substrate area and complicates the array beamforming network (BFN). Placing isolating hardware structures between antenna elements was also popularly studied [17], [18], [19], [20]. An intensive comparison of these hardware-based techniques for MIMO and SAR applications was performed in [21] and [22] from different aspects of performances. Popular techniques include decoupling networks [23], [24], neutralization line decoupling approaches [25], and pin-diode, varactor, and feeding line structure decoupling methods [26]. Some works also implemented periodic EM band-gap (EBG) structures [18], [27] to produce bandgap isolations at specific frequencies. It is also effective to design defected bandgap ground structures (DBGs) [17], [18], [19], [20], primarily consisting of different single-shaped parasitic structures with a resonance effect to catch the coupling energy.

Hsi-Tseng Chou and Rui-Zhe Wu are with the Graduate Institute of Communication Engineering, National Taiwan University, Taipei 10617, Taiwan (e-mail: chouht@ntu.edu.tw; r10942026@ntu.edu.tw).

Mobayode O. Akinsolu is with the Faculty of Arts, Science and Technology, Wrexham Glyndwr University, LL11 2AW Wrexham, U.K. (e-mail: m.akinsolu@glyndwr.ac.uk).

Yushi Liu and Bo Liu are with the School of Engineering, University of Glasgow, G12 8QQ Glasgow, Scotland (e-mail: 2109741L@glasgow.ac.uk; bo.liu@glasgow.ac.uk).

The common principle of these hardware-based techniques is to increase the mutual impedances to prevent power coupling. However, most have to sacrifice the operational frequency bandwidth and lack the generality to treat different situations as most are case-dependent and may have a physical limitation. The insufficiencies of the hardware-based isolation approaches can be improved by antenna radiation synthesis, owing to varying the array excitations. For example, Liu et al. [28] have used a differential evolution (DE) algorithm to alter the excitation waveforms and optimized the EEP of a time-modulated antenna array (TMAA).

Most past antenna array optimizations focused on radiation pattern synthesis in various application formats. They assumed identical antenna elements' patterns using IEPs and ignored the degradation of impedance matching by mutual coupling at the antenna elements' excitation ports. Even though the system degradation after synthesis can be estimated by multiplying the synthesized excitations with the inverse scattering matrix between the antenna elements, this procedure lacks the capability to assure proper system operation. Furthermore, the previous works have not considered the limits of reflected power to avoid RF device breakdowns for high-power radiation.

In this article, the radiation pattern synthesis incorporating the constraints of reflected power is proposed and examined. The novelty of this work is that the tradeoff of system performance and radiation patterns is performed during the synthesis. This software-based technique can relax the limitations of hardware-based methods to achieve broadband and wide-angle beam steering at a minimum cost. In this technique, the excitations of the antenna arrays, ignoring the mutual coupling effects, are first built to produce the desired radiation patterns, which serve as the target of radiation synthesis. Afterward, the cost functions of radiation targets incorporating the constraints of ARCs are defined and optimized by minimizing the difference between the desired antenna excitation weightings or gain patterns. The resulting radiation characteristics in gain, SLLs, and ARCs indicate a tradeoff between radiations and reflected power for system protection and interference avoidance.

The rest of this article is organized as follows. Section II describes the theoretical foundations of antenna radiations in the presence of mutual coupling influences. Section III describes the basic ARC concept and its roles in array radiations. The cost functions of different system considerations are discussed with optimization algorithms. Numerical examples based on HFSS simulations are shown in Section IV to validate the feasibility. Finally, a short remark and future works are discussed in Section V as a conclusion.

II. THEORETIC FOUNDATION FOR ANTENNA ARRAY RADIATION UNDER MUTUAL COUPLING INFLUENCES

A. Basic Concept of Mutual Coupling Between Array Elements

Consider an active antenna array, as illustrated in Fig. 1, to radiate directional or contoured beams. For compact interelement spacing and avoiding grating lobes in wide-angle beam steering, strong mutual coupling between antennas may exist
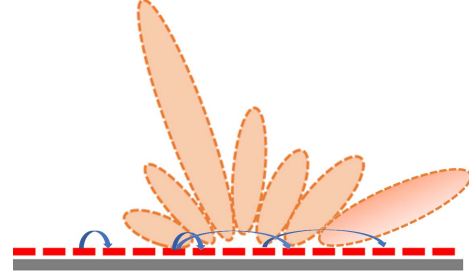

Fig. 1. Radiation scenario of active antenna arrays is shown with mutual coupling between antenna elements, which degrades the reflection coefficients.
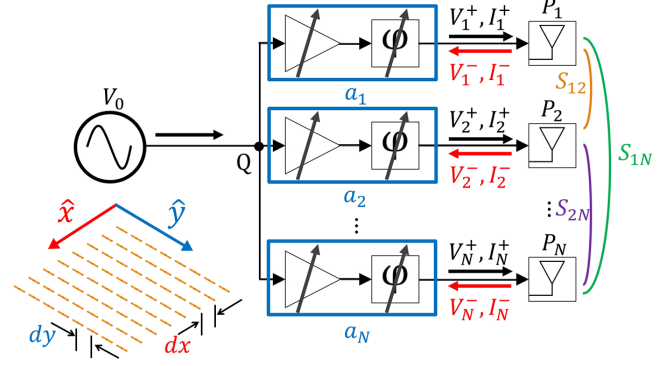

Fig. 2. Block diagram of active antenna array system with mutual coupling.

and degrade the radiation performance to cause scan blindness or RF device breakdown. Let the array of N antenna elements have excitations, $A_{1 \times N} = [a_n(n = 1 \sim N)]$, and let the scattering matrix (or called cross-coupling coefficients [5]) of mutual coupling between antenna elements be represented by S as

$$S_{N \times N} = [s_{nm}] = \begin{bmatrix} s_{11} & s_{12} & \cdots & s_{1(N-1)} & s_{1N} \\ s_{21} & s_{22} & \cdots & & s_{2N} \\ \vdots & \vdots & \ddots & & \vdots \\ s_{(N-1)1} & & \cdots & & s_{(N-1)N} \\ s_{N1} & s_{N2} & \cdots & s_{N(N-1)} & s_{NN} \end{bmatrix}. \tag{1}$$

Assume the BFNs consist of RF power splitters/combiners to produce single-port excitations by active RF feeding devices of phase shifters, power/low-noise amplifiers, and attenuators to control the excitation amplitudes and phases for the system operations, as shown by the system diagram in Fig. 2.

The radiation from the array can be expressed as

$$\bar{E}_{tot}(\bar{r}) = \sum_{n=1}^{N} a_n \bar{E}_n(\bar{r}) \tag{2}$$

where $\bar{E}_n(\bar{r})$ is the nth element's radiation with its excitation amplitude and phase being $|a_n|$ and $\phi_n = \angle a_n$, respectively. Under a perfect impedance matching at the antenna ports and without mutual coupling effects, these weightings excite the antenna ports, where $(V_n^-, I_n^-) = 0$ in Fig. 2 at the transmitting mode. In this case, $\bar{E}_n(\bar{r})$ is the IEP, $\bar{E}_{n,IEP}(\bar{r})$, of a standing-alone antenna element, obtained from a full-wave simulation.
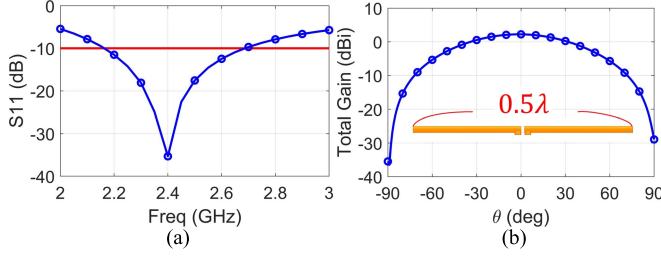
Fig. 3. Reflection coefficients and radiation patterns of a dipole antenna. (a) S_{11}. (b) Gain pattern ($\phi = 90°$).

Fig. 4. Comparison of the radiation patterns of the 4×4 antenna array. (a) H-plane ($\phi = 0°$). (b) E-plane ($\phi = 90°$).

Fig. 5. Comparison of the radiation patterns of the 8×8 antenna array. (a) H-plane ($\phi = 0°$). (b) E-plane ($\phi = 90°$).

It is noted that the radiation power density of the nth antenna element has the following relationship:

$$P_{rad,n}(\bar{r}) \propto |a_n E_n(\bar{r})|^2. \tag{3}$$

When the mutual coupling and the scattering matrix in (1) exist due to imperfect impedance matching, the radiation becomes

$$\bar{E}_{tot}(\bar{r}) = \sum_{n=1}^{N} a_n \bar{E}_{n,EEP}(\bar{r}) \tag{4}$$

where $\bar{E}_{n,EEP}(\bar{r})$ is the EEPs obtained from the IEP by [4]

$$\bar{E}_{n,EEP}(\bar{r}) = (1 + \Gamma_n)\bar{E}_{n,IEP}(\bar{r}) \tag{5}$$

where Γ_n is the ARC at the nth antenna's port defined by

$$\Gamma_n \frac{V_n^-}{V_n^+} = \frac{1}{a_n}\sum_{m=1}^{N} s_{nm}a_m = \frac{1}{V_n^+}\sum_{m=1}^{N} s_{nm}V_m^+. \tag{6}$$

Note that (6) can be simplified for the directional beam from a periodic array excited by uniform amplitudes. The excitations for a 1-D array to radiate the qth beam are

$$a_{n,q} = ce^{j\frac{2\pi}{N}(n-1)(q-1)}. \tag{7}$$

In this case, the ARC can be expressed as

$$\Gamma_{n,q} = e^{-j\frac{2\pi}{N}(n-1)(q-1)}\sum_{m=1}^{N} s_{nm}e^{j\frac{2\pi}{N}(m-1)(q-1)} \tag{8}$$

which is the discrete Fourier transform of the scattering matrix.

B. Mutual Coupling Influence on the Array Radiation by Examining the Behaviors of EEP Compositions

In this section, the behaviors of EEPs using them to form the array radiations are compared to the HFSS simulations. To produce strong EM mutual couplings, we consider arrays of 4×4 and 8×8 $\lambda/2$ dipoles with the dipoles' orientations in the y-direction on the xy plane, as shown by the inset in Figs. 2 and 3. The interelement separations are 0.75λ at 2.4 GHz. The single dipole's reflection coefficients and gain pattern on the yz plane are shown in Fig. 3(a) and (b), respectively, where S_{11} at the center frequency, 2.4 GHz, is -35.32 dB, and the bandwidth is 0.53 GHz from 2.16 to 2.68 GHz. The peak gain is 2.22 dBi. Note that using EEPs to resemble the radiation with EM mutual coupling removes the need for sophisticated and time-cumbersome full-wave simulations. It is valid for sm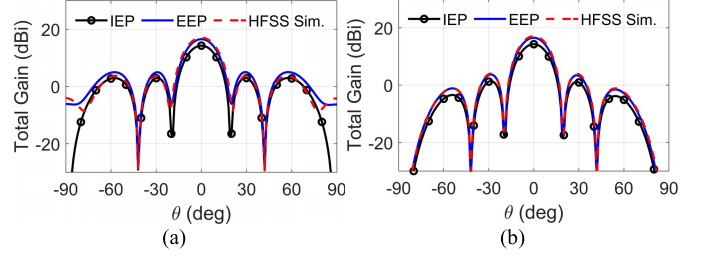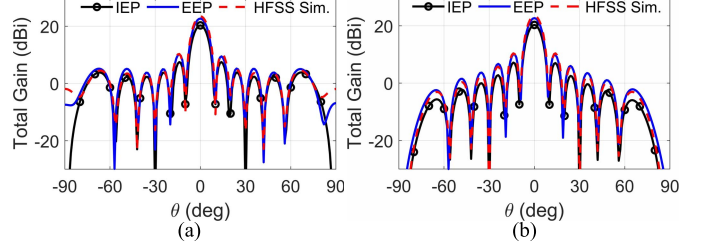all antennas operating at a single fundamental mode, where the current distributions on the antenna bodies are not significantly altered. The discrepancy will be very slight and limited.

The radiation patterns of these two arrays are shown in Figs. 4 and 5, respectively, where three solutions are shown for comparison. Denoted by "IEP" is the case using IEPs and array factor to find the array radiation pattern. The second is numerically exact (denoted by "sim"), obtained from the HFSS full-wave simulation on the entire dipole array. On the other hand, the third (indicated by "EEP") is the radiation pattern using the EEPs in Section II-A, which corrects the array radiations by incorporating the scattering matrix. It is seen that the EEP-based radiation patterns have an excellent agreement with the exact patterns in the main lobe and the first few sidelobes. The discrepancy appears at wide-angle beams. These behaviors happen to most antenna array cases because the antenna elements have smaller sizes of less than $\lambda/2$ to produce an exemplary array configuration.

III. INCORPORATION OF ARCs INTO THE COST FUNCTIONS OF RADIATION OPTIMIZATION

In this section, the radiation pattern synthesis incorporating the constraints of ARCs is presented with a focus on describing the implementation procedure and effective buildups of cost functions. Note that the radiation characteristics of an antenna array can be specified by examining the radiation patterns or the excitation weightings for the selected antenna types.

In the synthesis procedure, one first excludes the mutual-coupling effects and produces a set of excitation coefficients, $\tilde{A}_{1 \times N} = [\tilde{a}_n(n = 1 \sim N)]$, to radiate a set of EM far-field patterns $\tilde{G}(\theta, \phi)$. These $\tilde{A}_{1 \times N}$ and $\tilde{G}(\theta, \phi)$, as well as the subsequent SLLs, serve as the targeted specifications to be achieved by the EM optimization when the mutual-coupling influences exist. In addition, the reflection coefficients or

the reflected power at the excitation ports serve as another specification for optimization.

A. Constraint of ARC at the Combined Input Port of BFN

The architecture is illustrated in Fig. 2, where the ARC is defined at the port, Q, which inputs the BFNs (referred to as the B-ARC, hereafter). Let us assume that the BFN has good impedance matching to examine the effects of antenna reflection coefficients and mutual coupling. Thus, the net B-ARC can be defined by

$$\Gamma_{BFN} = \frac{A_{1\times N} S_{N\times N} A_{1\times N}^T}{A_{1\times N} A_{1\times N}^H} \qquad (9)$$

where the superscript "T" denotes the matrix transpose with "H" being the matrix Hermitian. The net power reflected back to the system from the BFN has the following relationship:

$$P_{refl} \propto \left| A_{1\times N} S_{N\times N} A_{1\times N}^T \right|^2. \qquad (10)$$

The minimization target intends to make $P_{refl} \to 0$, while retaining the radiation performance in (2) without causing severe degradation. A quasi-analytic solution is searched by defining a cost function that correlates the EM coupling interferences with the deviation of excitation weightings by

$$\Omega_1 \equiv \left| \tilde{A}_{1\times N} - A_{1\times N} \right|^2 + \alpha\left(A_{1\times N} S_{N\times N} A_{1\times N}^T\right)$$
$$+ \alpha^*\left(A_{1\times N} S_{N\times N} A_{1\times N}^T\right)^* \qquad (11)$$

where $\tilde{A}_{1\times N}$ and $A_{1\times N}$ are the desired and varying ones for optimization to minimizing the cost function. In (11), the complex weighting factor, α, is introduced to compromise the weight between P_{refl} and the excitation coefficients' deviations, which benefits the search for the quasi-analytic solution. One can vary α to minimize the cost function in (11). This quasi-analytic procedure is not automatic iterations but provides closed-form formulations in the optimization. One may conveniently plot the cost function to α. In (11), the first term is related to minimize radiation pattern deviation from the desired one by reducing the excitation deviation. The second and third terms are associated with the B-ARC minimization in the field strength scale. The goal is to minimize the B-ARCs at minimum radiation deviations. One can specify a constraint of maximum gain drop and then employ (11) to search for the solutions that reduce the B-ARC. It is clear that a larger $|\alpha|$ will cause a more significant beam deviation and performance degradation. It is desirable to keep $|\alpha|$ as small as possible.

With each $|\alpha|$ being a constant, (11) is minimized by taking the derivatives of (11) to $A_{1\times N}$, where the solution can be found by solving the zero derivatives, given as

$$A_{1\times N}$$
$$= \left(\tilde{A}_{1\times N} - \alpha^* \tilde{A}_{1\times N}^* \left(S_{N\times N}^H + S_{N\times N}^*\right)\right)$$
$$\times \left(I_{N\times N} - |\alpha|^2 \left(S_{N\times N}^H + S_{N\times N}^*\right)^* \left(S_{N\times N}^H + S_{N\times N}^*\right)\right)^{-1} \qquad (12)$$

where "$*$" is the complex conjugate. Equation (12) consists of two terms. The ones associated with α arise from the mutual couplings between antenna elements and are related to

the excitations of the influencing antennas and the scattering matrix. As mentioned earlier, one varies α and employs (12) to find the minimum Ω_1 in (11) in a tradeoff fashion. In the meantime, one also plots the radiation patterns and B-ARCs as indicators to select the optimum excitations until the tradeoff results are found. Note that minimizing (11) may not be the optimum solution to minimize (9) within the constraint of radiation performance. When $|\alpha|$ in (12) is too large, $A_{1\times N}$ will reduce to $\tilde{A}_{1\times N}^*$ after the unit-power normalization, resulting in an imaged radiation pattern to the original one. Thus, observing the variation of (9) within the radiation degradation constraint, one may pick the desired array excitations at a small $|\alpha|$.

B. Constraint of ARCs at the Individual Antenna Ports

The ARCs at the individual antenna ports, $P_n (n = 1 \sim N)$, (referred to as the A-ARCs, hereafter) are shown in (6), which serve as the constraints in the cost function to avoid RF devices breakdowns in the BFN. It is noted that (6) can be alternatively expressed in a matrix form, $\tilde{\Gamma} = [\Gamma_n (n = 1 \sim N)]$ by

$$\tilde{\Gamma} = A_{1\times N} S_{N\times N} ./ A_{1\times N} \qquad (13)$$

where "./" denotes the elemental division commend provided in MATLAB software. One extends the basic concept in (11) to define the cost function by

$$\Omega_2 \equiv \frac{|A_{1\times N} - \tilde{A}_{1\times N}|^2}{A_{1\times N} A_{1\times N}^H} + \alpha \max\{abs(A_{1\times N} S_{N\times N} ./ A_{1\times N})\} \qquad (14)$$

where the "abs" finds the absolute value of each element. This cost function is minimized to achieve the desired radiation based on the desired excitations. Again, the first term in (14) reduces the radiation deviation, while the second term picks the maximum A-ARC among the antenna ports first and then minimizes it. α is a positive real number used to balance the weightings between these two terms. Similar to Section III-A, one intends to obtain a tradeoff solution to achieve good radiation patterns and A-ARCs at the antenna ports. Methods, such as the quasi-Newton method [29] and the relative interpretation, can be used to solve it. The function code "fminunc" in MATLAB Tool Box [30] can be used to optimize this cost function.

C. Optimization of Antenna Gain, SLLs, and ARCs at the Antenna Ports

The optimization of radiation patterns and A-ARCs in Section III-B can also be applied to incorporate the antenna radiation pattern directly. Thus, the cost function, Ω_2, in (14) is alternatively expressed in the following form:

$$\Omega_3 = \max\{-(G_{dB} - \tilde{G}_{dB}), 0\} + \max\{(\max(\tilde{\Gamma}_{dB}) - \Gamma_{spec}), 0\}$$
$$+ \max\{(SLL_{dB} - SLL_{spec}), 0\} \qquad (15)$$

where Γ_{spec} and SLL_{spec} denote the system specified allowable levels of A-ARCs and SLLs in the decibel scales. Here, the SLLs are computed relative to the peak gain, G_{dB}. The values of G_{dB} and $\tilde{G}_{dB}$ are the calculated and desired peak

gains along the desired beam direction in the decibel scales. Both G_{dB} and SLL_{dB} are computed in the presence of mutual coupling, i.e., from the EEPs to form the beams. The comparison with "0" is set intentionally for a convenient coding purpose to do the justification of optimization. It is noted that each term in (15) takes the largest value between it and 0, making $\Omega_3 = 0$ when the optimized results fulfill all the specifications. Appropriate specifications are needed to avoid overoptimization in some extreme cases. For example, an unreasonably large beamwidth can also reduce SLL.

The optimization of (15) does not have closed-form solutions to perform the iterations. Moreover, a reasonably high-quality initial solution cannot be easily specified as the starting point for performing the optimization algorithms. It is noted that local optimization techniques like that addressing (14) may easily get trapped in the local optima and fail to satisfy the multiple specifications of peak gains, A-ARCs, and SLLs in (15). In this work, we propose to employ the DE algorithm [31], [32], which is a global optimization method widely used for antenna design optimization [33]. Its operators have also been employed to develop the state-of-the-art artificial intelligence (AI)-driven antenna design algorithms (e.g., [34] and [35]).

The implementation of DE first specifies a population P of Q decision variables (i.e., the array excitations) to iteratively search for optimum solutions. Let $\bar{x} = (x_1, \ldots, x_Q) \in R^Q$ be an individual solution of excitations in P. The DE procedure generates child solutions from P by mutation and crossover operations. In particular, the mutation produces a donor vector, $\bar{v}$, from individuals in P, which is one-to-one correspondence to $\bar{x}$. Several mutation strategies, trading off between the population diversities (i.e., the ability to avoid being trapped in local optima) and convergence speed, have been examined in the past [32]. In this article, the DE/rand-to-best/1 mutation strategy [31] is employed, which gives

$$\bar{v}^i = \bar{x}^i + F\left(\bar{x}^{best} - \bar{x}^i\right) + F\left(\bar{x}^{r_1} - \bar{x}^{r_2}\right) \quad (16)$$

where $\bar{x}^i$ is the ith individual solution of P (the current population), and $\bar{x}^{best}$ is the individual in P with the best cost function value. In (16), $\bar{x}^{r_1}$ and $\bar{x}^{r_2}$ are two additional mutually exclusive solutions randomly selected from P, which are different from $\bar{x}^{best}$ and $\bar{x}^i$. $F \in (0, 2]$ is the scaling factor. Thus, $\bar{v}^i$ is the ith mutant vector that can be used to generate the child solution, $\bar{u} = (u_1, \ldots, u_Q) \in R^Q$, through a crossover operation. A variable index, $j_{rand} \leq Q$, is randomly selected. A uniformly distributed random number, r_a, is generated to produce the offspring element

$$u_j = \begin{cases} v_j, & \text{if } r_a \geq CR | j = j_{rand} \\ x_j, & \text{otherwise} \end{cases} \quad (17)$$

where $CR \in [0, 1]$ is the crossover rate. Then, a one-to-one-based greedy selection between $\bar{u}^i$ and $\bar{x}^i$ is carried out considering the cost function values, generating the population for the next iteration. In this work, the population size is 90, with $F = 0.8$ and $CR = 0.9$. The maximum number of iterations is set by 10 000.
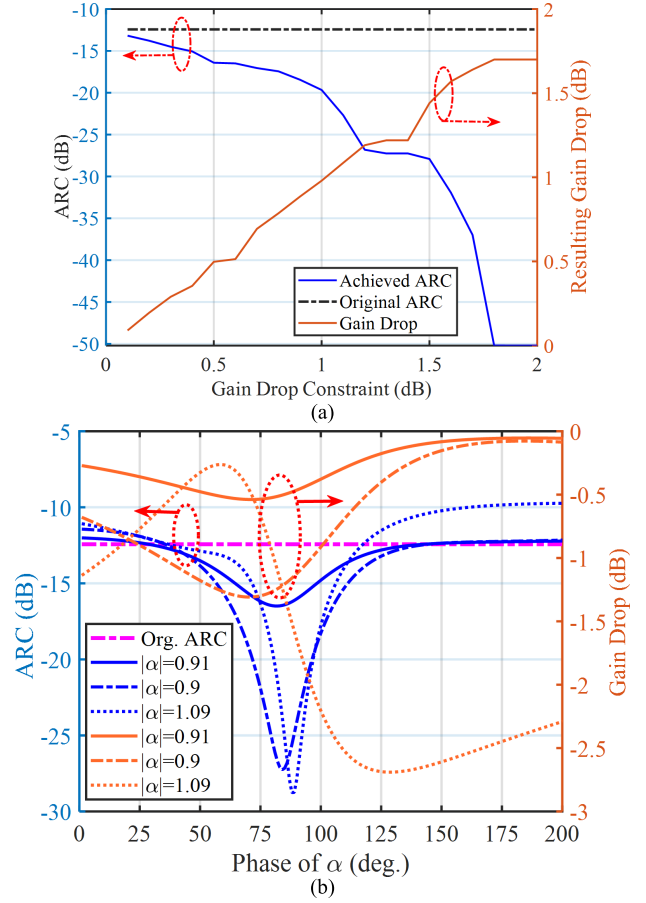

Fig. 6. Variations of B-ARCs and gain drops to the gain drop constraints and α variations. (a) B-ARC and gain drop versus gain drop constraint. (b) B-ARC and gain drop versus α.

IV. NUMERICAL EXAMINATIONS FOR VALIDATION

Numerical examples validate the proposed techniques' feasibility and effectiveness, where HFSS simulations are employed to produce the results.

A. Constraint of B-ARC and Radiation Degradation at the Combined Input Port of BFN

This examination considers an array of 8×8 microstrip patch antennas implemented on an FR4 dielectric substrate ($\varepsilon_r = 4.4$, $\tan \delta = 0.02$, and 1.6 mm in thickness). The period of array elements on both dimensions is $\lambda/2$ at 2.5 GHz. The scattering matrix was obtained from the HFSS full-wave simulations and is embedded to compute the radiation patterns. Directional beams are considered for easy demonstration. The main beams' maximum gain drops were set as a constraint to optimize the cost function in (11), which was achieved by varying the complex α, such that (9) is minimized.

One first considers a broadside beam with uniform amplitudes and phases for the original excitations, $\tilde{A}_{1 \times N}$. The optimum results were obtained by altering the amplitudes and phases of α. For each α, $A_{1 \times N}$ was obtained from (12) and then employed to find the B-ARC in (9) and the array antenna gain to compute the gain drops. The constraint of the maximum gain drop was specified. Thus, one can search
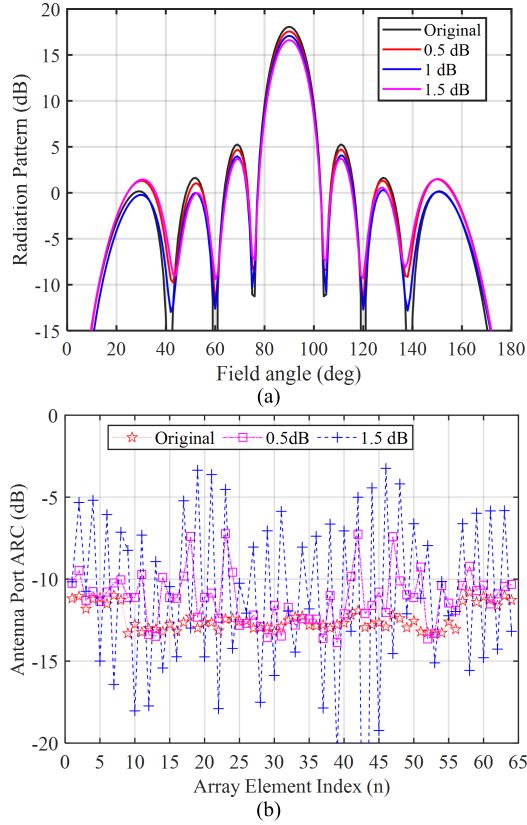
Fig. 7. Variation of radiation patterns and the A-ARCs at the antenna ports due to the B-ARC optimizations. (a) Radiation pattern comparison. (b) Antenna port A-ARCs.

the value of α to minimize the B-ARC under the gain drop constraint. A larger range of gain drop constraints will result in a smaller B-ARC, as shown in Fig. 6, where the achievable minimum B-ARCs under the range of gain drop constraints are plotted. Fig. 6(a) also indicates the B-ARC by the original uniform array excitation to compare the B-ARC improvement. The achieved gain drops are also shown in Fig. 6(a), where a relatively linear variation has been obtained. Compared to the reference B-ARC, the achieved minimum B-ARCs follow the increase of gain drop constraint even though they are not linear.

Fig. 6(b) shows the behaviors of the B-ARCs and gain drops to the α variations, where the three cases of $|\alpha|$ correspond to the three cases of gain drop constraints by 0.5, 1, and 1.5 dB.

The curves were plotted to the phase variations of α, where the blue curves are the B-ARC variations, while the orange curves are the actual gain drops. Comparing the curves of these two colors shows the relationship between gain drops and B-ARC reductions. One can pick the proper values of B-ARCs and gain drops fulfilling the system requirements, which allows one to determine the value of α, which is afterward substituted into (12) to find the optimum excitation $A_{1 \times N}$. Numerical results show that there is a limit of minimum B-ARC. In practical applications, one may select tradeoff results of gain drop and ARCs from Fig. 6(a) to fulfill the system requirement.

Fig. 7(a) shows the resulting radiation patterns for the three cases of gain drop constraints by 0.5, 1, and 1.5 dB compared

to the reference result of uniform excitations. All excitations were normalized to a unit power. It is seen that the gain drops are similar to the applied constraints. The SLLs are slightly reduced on the first few sidelobes, which do not get worse by these gain degradations.

On the other hand, the resulting A-ARCs at the antenna feeding ports are shown in Fig. 7(b). The red star symbols are the reference results of uniform excitations for comparison. The square and plus symbols represent the A-ARCs for the two cases of gain drop constraints by 0.5 and 1.5 dB, respectively. In these cases, the B-ARCs at the BFN's I/O port are −16.41 and −27.91 dB, as shown in Fig. 6(a), where the reference B-ARC is −12.2 dB. The B-ARC optimizations increase the variations of A-ARCs. A more significant B-ARC reduction requirement may result in a larger variation of A-ARCs at the antenna ports.

They are alternatively improved and worsened. Some of them may degrade to −3 dB at the antenna ports for the case of a 1.5 dB gain drop constraint (or −27.91 dB B-ARC at the BFN port).

One next considers a 150° beam-steering case. Fig. 8(a) shows the B-ARC and gain drop variations to α, where $|\alpha| = 0.32$ was obtained for the cases of gain drop constraints smaller than 1.5 dB. The beam steering has reduced the B-ARC compared to the previous case in Fig. 6 when the original uniform excitations are employed. In this synthesis, the gain drop is less than 0.16 dB, which can produce a B-ARC by −64 dB, more than 45 dB improvement. The resulting radiation patterns are shown in Fig. 8(b), where the two patterns almost overlap, showing neglectable radiation degradation.

On the other hand, the antenna ports' A-ARCs are demonstrated in Fig. 8(c). It is first seen that the A-ARCs become worse in comparison to the broadside beam case in Fig. 7(b), even when one uses the original uniform excitations. The A-ARCs can be as large as −5.5 dB. It is also seen that when the optimization is applied, the variation of A-ARC becomes larger. Most of them are improved compared to the broadside beam case in Fig. 7 due to the insignificant gain drop or pattern distortion. It is seen that the A-ARCs always get worse when the mutual coupling effects are considered. These poor A-ARC performances may cause RF component breakdowns when the RF devices are installed directly behind the antennas.

B. Constraint of A-ARCs at the Individual Antenna Ports

The examination considers the array of 8×8 dipoles in Section II-B and Fig. 2, where the periods are 0.5λ at 2.4 GHz.

Compared to (11), (14) selects the worst A-ARC (maximum) to minimize the cost function, where α is set by a positive value for simplification. One first considers a broadside beam and optimizes the A-ARCs via (14), where $\tilde{A}_{1 \times N}$ is the Dolph–Chebyshev distribution. Fig. 9(a)–(d) shows the achieved gain drops, SLLs, beam deviations, and the maximum A-ARCs, respectively, for $0 < \alpha < 40$, where $\alpha = 0$ is the case of uniform excitations without optimization. The worst A-ARCs are larger than −8 dB. After optimization, the cases of gain drop also reduce SLLs, where the gain drops are less than 0.03 dB, while the SLLs have improvements of almost
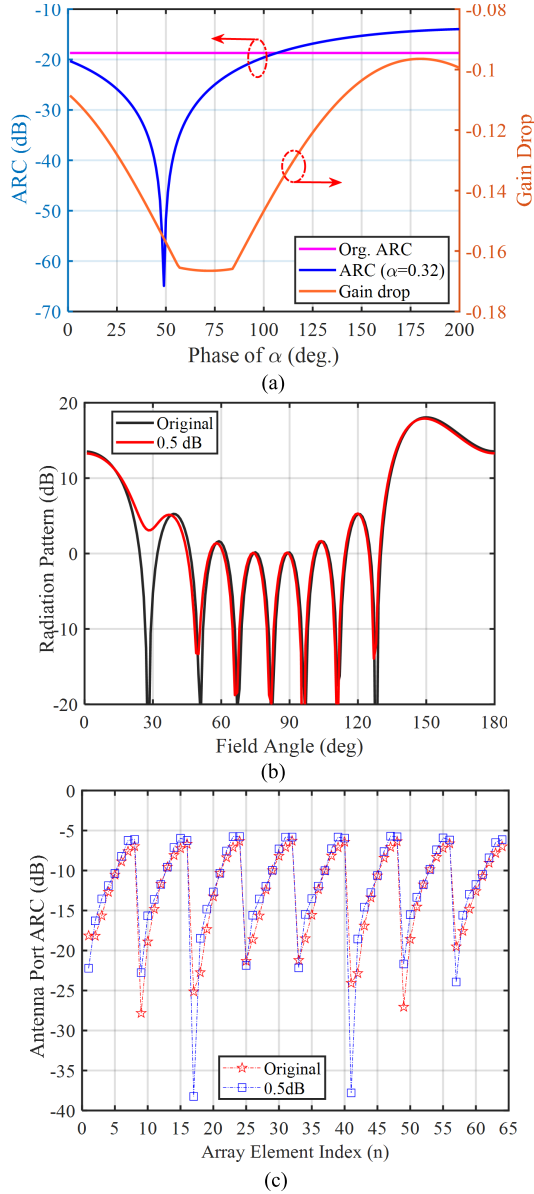
Fig. 8. BFN B-ARC and gain drop variations are shown in (a). The radiation patterns and the A-ARCs at the antenna ports due to the B-ARC optimizations are shown in (b) and (c). (a) B-ARC and gain drop versus α. (b) Radiation pattern comparison. (c) Antenna port A-ARCs.

0.8 dB. In these cases, the beam directions remain stably unaltered. However, the maximum A-ARCs are improved by more than 2 dB to make them smaller than -10 dB.

One next considers the $(\theta, \phi) = (30°, 60°)$ beam scan case. The radiation behaviors are shown in Fig. 10(a)–(d) with respect to Fig. 9(a)–(d). In this case, the maximum A-ARCs degrade to -6.1 dB from -7.7 dB. The gain drops are smaller than 0.02 dB, but the SLLs are improved by more than 1.2 dB. The maximum A-ARCs are enhanced by more than 2 dB. Compared to Fig. 9(d), the improvement of maximum A-ARCs is more complex, but the improved values are larger.

C. Optimization of Antenna Gain, SLLs, and A-ARCs at the Antenna Ports

One employs (15) to optimize the radiation patterns and A-ARCs, compared with those using (14) in Section IV-B.
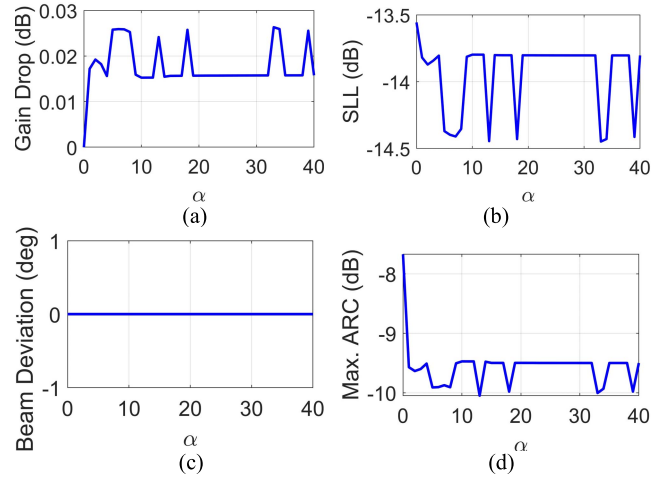

Fig. 9. Resulting radiation characteristics and maximum A-ARCs after optimization by altering α for a broadside beam. (a) Gain drop. (b) SLL. (c) Beam deviation. (d) Maximum A-ARCs.
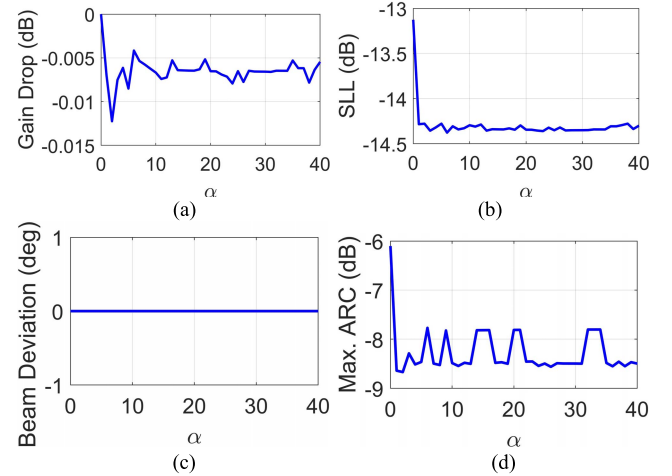

Fig. 10. Resulting radiation characteristics and maximum ARCs after optimization by various α for the $(\theta, \phi) = (30°, 60°)$ beam direction. (a) Gain drop. (b) SLL. (c) Beam deviation. (d) Maximum A-ARCs.

In these examinations, various goals of gains, SLLs, and A-ARCs are set, where the antenna array fed by the Dolph–Chebyshev distributions (denoted by "Dol" in the numerical results and figures) for the target SLLs is used as comparison references. The results obtained using (14) as the cost function in Section IV-B are denoted by "Fmi."

Tables I and II summarize the achieved gains, SLLs, and maximum A-ARCs for the broadside and $(\theta, \phi) = (30°, 60°)$ beams, respectively. The "Fmi" cases usually take about 20–25 s CPU time, while the "Opt" cases need about 700–750 s. In Table I, the broadside beams consider two target SLLs of -20 and -15 dB. Before the optimizations, the resulting maximum A-ARCs are -9.03 and -7.67 dB, respectively, larger than the popular -10 dB threshold. The SLLs are -18.56 and -13.56 dB for the two reference excitations. One first applies (14) to optimize the maximum A-ARCs, which do not involve the SLL suppression. Table I shows that the gains remain similar to the nonsynthesized ones, while the
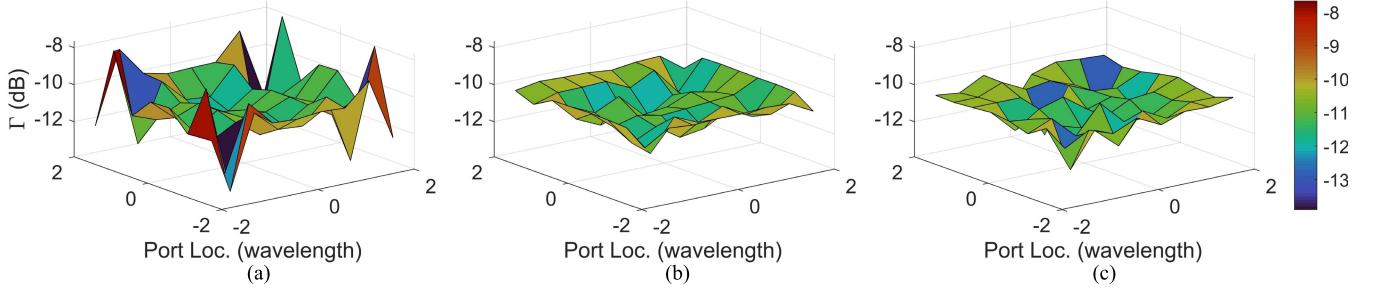
Fig. 11. A-ARCs by different approaches in Table I for the broadside beam. (a) Dol. 2. (b) Fmi. 1. (c) Opt. 5.
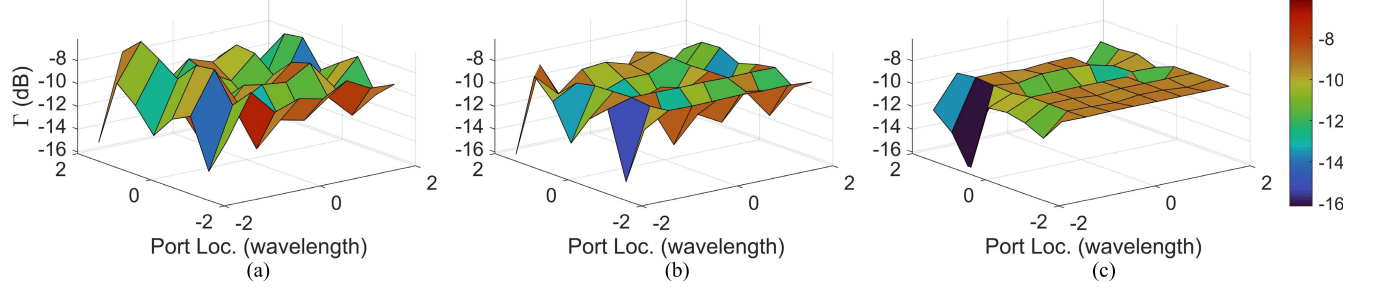

Fig. 12. A-ARCs by different approaches in Table II for the steered beam. (a) Dol. 1. (b) Fmi. 1. (c) Opt. 1.

TABLE I
BROADSIDE BEAM OPTIMIZED RESULTS

| Case | Input Parameter and Result (Unit: dB) | | | | |
	Specification	Gain	SLL	Max. ARC	Cost
Dol. 1	SLL = -20	19.33	-18.56	-9.03	
Dol. 2	SLL = -15	19.63	-13.56	-7.67	
Fmi. 1	SLL = -20	**19.33**	**-18.96**	**-10.31**	
Fmi. 2	SLL = -15	**19.67**	**-14.44**	**-10.05**	
Opt. 1	(G, SLL, ARC) =(19.5,-20,-10)	**19.15**	**-19.64**	**-10.00**	**0.36**
Opt. 2	(G, SLL, ARC) =(19,-20,-10)	19.00	-19.72	-10.09	0.28
Opt. 3	(G, SLL, ARC) =(19,-20,-15)	18.70	-19.78	-10.55	4.98
Opt. 4	(G, SLL, ARC) =(19,-15,-10)	19.00	-15.06	-10.01	0
Opt. 5	(G, SLL, ARC) =(19.5,-15,-10)	**19.50**	**-14.93**	**-10.00**	**0.07**
Opt. 6	(G, SLL, ARC) =(19,-15,-15)	19.00	-14.83	-10.36	4.81
Opt. 7	(G, SLL, ARC) =(18.5,-15,-15)	18.60	-14.96	-10.41	4.63

TABLE II
SCANNING BEAM $(\theta, \phi) = (30°, 60°)$ OPTIMIZED RESULT

| Case | Input Parameter and Result (Unit: dB) | | | | |
	Specification	Gain	SLL	Max. ARC	Cost
Dol. 1	SLL = -15	19.47	-13.13	-6.10	
Fmi. 1	SLL = -15	19.45	-14.28	-8.67	
Opt. 1	(G, SLL, ARC) =(19,-15,-10)	18.95	-14.98	-9.23	0.84
Opt. 2	(G, SLL, ARC) =(18,-15,-10)	18.13	-14.81	-9.15	1.04
Opt. 3	(G, SLL, ARC) =(19,-10,-10)	18.75	-11.75	-9.38	0.86

because beam steering may result in considerable A-ARC degradation. In this case, the achieved SLL is −13.13 dB, similar to the broadside beam case. However, the maximum A-ARC is −6.10 dB, which may incur strong reflected power for high-power radiations. It is seen that using (14) improves the SLL by 1.15 dB. The maximum A-ARC is −8.67 dB, a 2.57 dB improvement. In Table II, the optimization using (15) examines three cases. It is seen that the SLL performances are further improved. The A-ARC performances are also enhanced with values much closer to the −10 dB threshold. However, these slightly sacrifice the gain performance to achieve these results.

The resulting A-ARCs are shown in Figs. 11 and 12. In particular, Fig. 11(a)–(c) corresponds to "Dol. 2," "Fmi. 1," and "Opt. 5" cases in Table I, while Fig. 11(a)–(c) corresponds to "Dol. 1," "Fmi. 1," and "Opt. 1" in Table II. It is seen that without optimization, many A-ARCs are larger than −10 dB, especially in the beam steering case. After optimizations, they significantly improved, with most smaller than −10 dB.

SLLs have some improvements. The maximum A-ARCs are −10.31 and −10.05 dB, respectively, smaller than the −10 dB threshold and representing 1.3 and 2.38 dB improvements. In applying (15), various design goals are pursued. As shown in Table I, most cases can achieve the desired gains, where the achieved SLLs are also very close to the specified ones with less than 0.25 dB differences. The maximum A-ARCs of all cases are smaller than −10 dB. On the other hand, Table II summarizes the results for the $(\theta, \phi) = (30°, 60°)$ beam. Only one target "Dol" SLL of −15 dB is considered
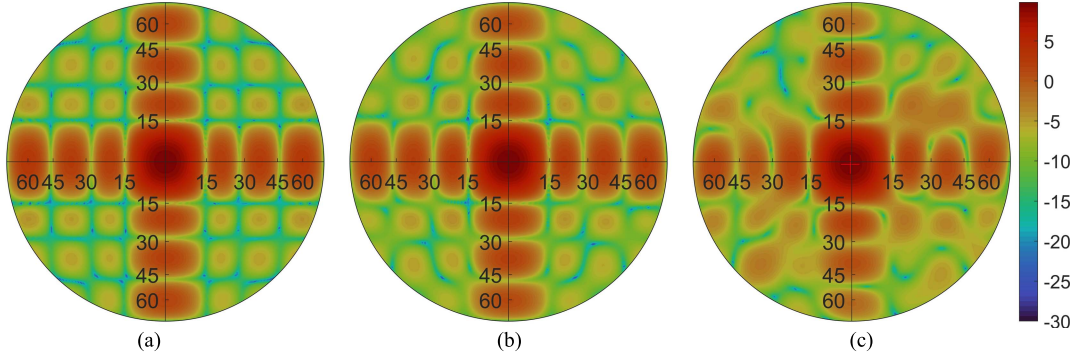
Fig. 13. Gain patterns in the u-v space by different approaches in Table I for the broadside beam. (a) Dol. 2. (b) Fmi. 1. (c) Opt. 5.
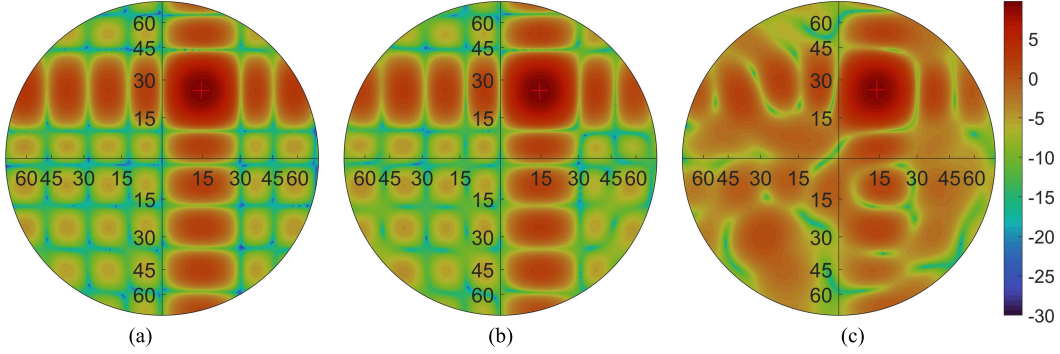

Fig. 14. Gain patterns in the u-v space by different approaches in Table II for the steered beam. (a) Dol. 1. (b) Fmi. 1. (c) Opt. 1.

The resulting radiation patterns are shown in Figs. 13 and 14 in the u-v space, corresponding to Figs. 11 and 12, respectively. It is seen that using (14) may better retain the radiation patterns much closer to the original ones before optimizations. Using (15) may redistribute the sidelobes away from the two orthogonal *xz* and *yz* planes. These sidelobe redistributions do not cause any problems because, in these nonprincipal planes, their SLL values are very low in the original cases. The redistributions do not significantly impact the overall SLLs.

Finally, one compares the frequency responses of radiations and the maximum A-ARCs for the two beams' synthesis, where the responses were synthesized at the sampled frequencies. The results are shown in Figs. 15 and 16 for the cases "Doi. 1," "Fmi. 1," and "Opt. 1" and "Doi. 1," "Fmi. 1," and "Opt. 1" in Tables I and II, respectively. "Dol. 1" has a better gain performance for the achieved gain variations in the broadside beam. "Fmi. 1" has a slight gain offset of 0.2–0.3 dB, almost constant in the frequency band. "Opt. 1" has the same gain as "Fmi. 1" at 2.5 GHz, but the gain degradation increases when the frequency is away from 2.5 GHz. The reason is the incorporation of SLLs in the optimization of using (15). Thus, the SLL responses in Fig. 15 show a better performance for "Opt. 1," which has the smallest except for the frequency at 2.2 GHz. Both "Fmi. 1" and "Opt. 1" have better improvements in the frequency band. Fig. 15 also shows good performance of very small beam deviations, less than 2.5°, by synthesizing (15). On the other hand, the maximum A-ARCs are all improved by the proposed synthesis
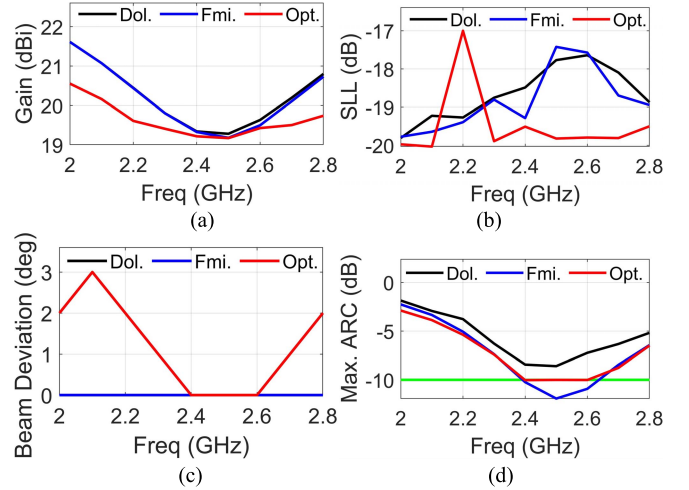

Fig. 15. Frequency responses of gain, SLL, beam deviation, and maximum ARCs by various approaches in Table I for the broadside beam. (a) Gain. (b) SLL. (c) Beam deviation. (d) Maximum A-ARCs.

using (14) and (15). The improvements are maximum at frequencies near 2.5 GHz.

The advantage of using (15) as the cost function becomes apparent for the steered beam, as shown in Fig. 16. It is seen that the proposed synthesis using (15) provides better frequency responses in gain and SLL, where the variations are minor, even though it results in more significant beam deviations when the frequencies are away from 2.5 GHz.
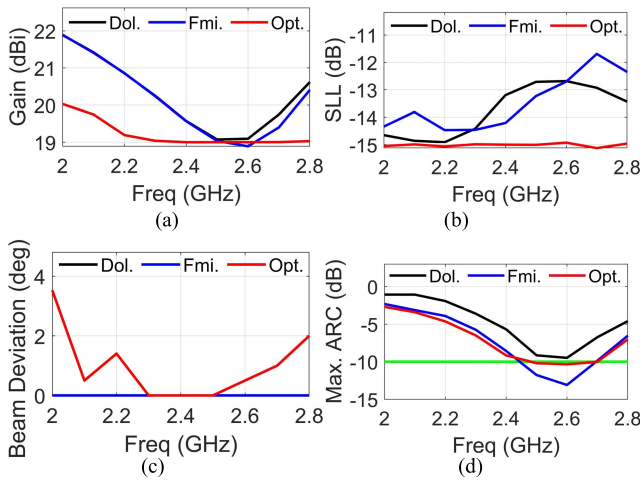
Fig. 16. Frequency responses of gain, SLL, beam deviation, and maximum A-ARCs by various approaches in Table II for the steered beam. (a) Gain. (b) SLL. (c) Beam deviation. (d) Maximum A-ARCs.

The SLLs are almost constant within the frequency band by using (15). The SLL results of "Fmi. 1" have more deviations at high frequencies because (14) does not incorporate the control of SLL in the optimization. In all cases of Figs. 15 and 16, the behaviors of A-ARCs have very narrow frequency bands, indicating that the synthesis should be performed at various desired frequencies.

V. CONCLUSION

Antenna array radiation synthesis incorporating the ARC constraints has been investigated, which considerably reduces reflected power, avoiding signal interferences and reducing the risk of system breakdown and scan blindness. Three scenarios and cost functions have been examined to study their behaviors and optimization mechanisms. Numerical results show that the ARCs can be reduced to a certain level in practical applications under a slight gain sacrifice. A proper setup of gain, SLL, and ARC goals can optimize the radiation characteristics. Various approaches to numerical optimizations have been implemented in these examinations with different advantages. The quasi-analytical solutions are applicable to reduce the ARCs at the BFN and antenna ports, which are computationally efficient but do not warrant a global optimization.

Moreover, when multiple objects of radiation optimization are desired, it is not easy to find a closed-form formulation. DE can be effective. It is seen that a suitable cost function can result in different degrees of optimization. Future works will attempt to improve the efficiency and effectiveness of radiation synthesis. Physical limitations will also be pursued.

REFERENCES

[1] P. Hannan, "The element-gain paradox for a phased-array antenna," *IEEE Trans. Antennas Propag.*, vol. AP-12, no. 4, pp. 423–433, Jul. 1964.
[2] W. Kahn, "Active reflection coefficient and element efficiency in arbitrary antenna arrays," *IEEE Trans. Antennas Propag.*, vol. AP-17, no. 5, pp. 653–654, Sep. 1969.
[3] R. C. Hansen, *Microwave Scanning Antennas: Antenna Theory and Practice*, vol. 2. New York, NY, USA: Academic, 1966.
[4] D. M. Pozar, "The active element pattern," *IEEE Trans. Antennas Propag.*, vol. AP-42, no. 8, pp. 1176–1178, Aug. 1994.
[5] C. A. Balanis, *Antenna Theory: Analysis and Design*, 4th ed. Hoboken, NJ, USA: Wiley, 2015.
[6] R. C. Hansen, *Phased Array Antennas*. Hoboken, NJ, USA: Wiley, 1998, ch. 7.
[7] D. F. Kelley, "Relationships between active element patterns and mutual impedance matrices in phased array antennas," in *Proc. IEEE Antennas Propag. Soc. Int. Symp.*, Jun. 2002, pp. 524–527.
[8] P. S. Kildal and K. Rosengren, "Electromagnetic characterization of MIMO antennas including coupling using classical embedded element pattern and radiation efficiency," in *Proc. IEEE Antennas Propag. Soc. Symp.*, Jun. 2004, pp. 1259–1262.
[9] D. F. Kelley, "Embedded element patterns and mutual impedance matrices in the terminated phased array environment," *Proc. IEEE Antennas Propag. Soc. Int. Symp.*, vol. 3A, pp. 659–662. Jul. 2005.
[10] R. Mailloux, *Phased Array Antenna Handbook*, 2nd ed. Norwood, MA, USA: Artech House, 2005.
[11] D. I. L. de Villiers and R. Maaskant, "Element pattern prediction in mutually-coupled arrays through isolated antenna characterization," in *Proc. Int. Symp. Antennas Propag. (ISAP)*, Oct. 2017, pp. 1–2.
[12] K. F. Warnick, D. B. Davidson, and D. Buck, "Embedded element pattern loading condition transformations for phased array modeling," *IEEE Trans. Antennas Propag.*, vol. 69, no. 3, pp. 1769–1774, Mar. 2021.
[13] W. Wasylkiwskyj and W. Kahn, "Scattering properties and mutual coupling of antennas with prescribed radiation pattern," in *Proc. IEEE Antennas Propag. Soc. Int. Symp.*, Dec. 1969, pp. 154–160.
[14] D. M. Pozar, *Microwave Engineering*, 4th ed. New York, NY, USA: Wiley, 2005.
[15] J. Tao and Q. Feng, "Compact UWB band-notch MIMO antenna with embedded antenna element for improved band notch filtering," *Prog. Electromagn. Res. C*, vol. 67, pp. 117–125, 2016.
[16] R. Karimian, M. Soleimani, and S. M. Hashemi, "Tri-band four elements MIMO antenna system for WLAN and Wimax application," *J. Electromagn. Waves Appl.*, vol. 26, nos. 17–18, pp. 2348–2357, Dec. 2012.
[17] I. Chang and B. Lee, "Design of defected ground structures for harmonic control of active microstrip antenna," in *Proc. IEEE Antennas Propag. Soc. Int. Symp.*, Jun. 2002, pp. 852–855.
[18] J. Hua-Song, Q. Dong-Dong, R. Jia-Ren, Z. Peng, and D. R. Becerra, "Application of EBG and DGS structure on antenna array," in *Proc. Int. Conf. Image Anal. Signal Process.*, Nov. 2012, pp. 1–4.
[19] M. K. Khandelwal, B. K. Kanaujia, and S. Kumar, "Defected ground structure: Fundamentals, analysis, and applications in modern wireless trends," *Int. J. Antennas Propag.*, vol. 2017, pp. 1–22, Feb. 2017.
[20] A. Kumar, A. Q. Ansari, B. K. Kanaujia, J. Kishor, and L. Matekovits, "A review on different techniques of mutual coupling reduction between elements of any MIMO antenna. Part 1: DGSs and parasitic structures," *Radio Sci.*, vol. 56, no. 3, pp. 1–25, Mar. 2021.
[21] M. Alibakhshikenari et al., "A comprehensive survey on 'various decoupling mechanisms with focus on metamaterial and metasurface principles applicable to SAR and MIMO antenna system,'" *IEEE Access*, vol. 8, pp. 192965–193004, 2020.
[22] H. Tat Hui, "Decoupling methods for the mutual coupling effect in antenna arrays: A review," *Recent Patents Eng.*, vol. 1, no. 2, pp. 187–193, Jun. 2007.
[23] J. Andersen and H. Rasmussen, "Decoupling and descattering networks for antennas," *IEEE Trans. Antennas Propag.*, vol. AP-24, no. 6, pp. 841–846, Nov. 1976.
[24] K.-L. Wong, C.-Y. Tsai, and J.-Y. Lu, "Two asymmetrically mirrored gap-coupled loop antennas as a compact building block for eight-antenna MIMO array in the future smartphone," *IEEE Trans. Antennas Propag.*, vol. 65, no. 4, pp. 1765–1778, Apr. 2017.
[25] S.-W. Su, C.-T. Lee, and F.-S. Chang, "Printed MIMO-antenna system using neutralization-line technique for wireless USB-dongle applications," *IEEE Trans. Antennas Propag.*, vol. 60, no. 2, pp. 456–463, Feb. 2012.
[26] J.-H. Lim, Z.-J. Jin, C.-W. Song, and T.-Y. Yun, "Simultaneous frequency and isolation reconfigurable MIMO PIFA using PIN diodes," *IEEE Trans. Antennas Propag.*, vol. 60, no. 13, pp. 5939–5946, Dec. 2012.
[27] S. Ghosh, T.-N. Tran, and T. Le-Ngoc, "Dual-layer EBG-based miniaturized multi-element antenna for MIMO systems," *IEEE Trans. Antennas Propag.*, vol. 62, no. 8, pp. 3985–3997, Aug. 2014.

[28] Y. Liu, J. Bai, J. Zheng, H. Liao, Y. Ren, and Y. J. Guo, "Efficient shaped pattern synthesis for time modulated antenna arrays including mutual coupling by differential evolution integrated with FFT via least-square active element pattern expansion," *IEEE Trans. Antennas Propag.*, vol. 69, no. 7, pp. 4223–4228, Jul. 2021.

[29] D. F. Shanno, "Conditioning of quasi-Newton methods for function minimization," *Math. Comput.*, vol. 24, no. 111, pp. 647–656, 1970.

[30] (2021). The MathWorks I. *Optimization Toolbox*. Natick, MA, USA. [Online]. Available: https://www.mathworks.com/help/optim/

[31] R. Storn, "On the usage of differential evolution for function optimization," in *Proc. North Amer. Fuzzy Inform. Process. Soc.*, Jun. 1996, pp. 519–523.

[32] K. Price, R. Storn, and J. Lampinen, *Differential Evolution: A Practical Approach to Global Optimization*. Berlin, Germany: Springer, 2005.

[33] P. Rocca, G. Oliveri, and A. Massa, "Differential evolution as applied to electromagnetics," *IEEE Antennas Propag. Mag.*, vol. 53, no. 1, pp. 38–49, Feb. 2011.

[34] B. Liu, H. Aliakbarian, Z. Ma, G. A. E. Vandenbosch, G. Gielen, and P. Excell, "An efficient method for antenna design optimization based on evolutionary computation and machine learning techniques," *IEEE Trans. Antennas Propag.*, vol. 62, no. 1, pp. 7–18, Jan. 2014.

[35] B. Liu et al., "An efficient method for complex antenna design based on a self adaptive surrogate model-assisted optimization technique," *IEEE Trans. Antennas Propag.*, vol. 69, no. 4, pp. 2302–2315, Apr. 2021.

Rui-Zhe Wu received the B.S. degree in electrical engineering from National Taiwan University, Taipei, Taiwan, in 2021, where he is currently pursuing the master's degree under the supervision of professor Hsi-Tseng Chou.

His current research interests include antenna theory about antenna-in-package, lens antenna, phased array, and its beamforming optimization skills.

Mobayode O. Akinsolu (Senior Member, IEEE) received the M.Sc. degree (Hons.) in electrical and electronic engineering from the University of Bradford, Bradford, U.K., in 2014, after his undergraduate studies and compulsory national service in Nigeria.

He then worked as a Research Fellow (Industrial Attaché) and a Visiting Researcher at the National Space Research and Development Agency, Abuja, Nigeria, and the RFID Research Centre, African University of Science and Technology, Galadima, Nigeria, respectively, until 2016. From 2016 to 2019, he was a Ph.D. scholarship awardee in recognition of a joint project between Wrexham Glyndwr University, Wrexham, U.K., and the University of Birmingham, Birmingham, U.K. His Ph.D. research focused on electromagnetic design automation using surrogate model-assisted evolutionary algorithms and he received a commendation from the University of Chester, U.K., for the publications record (more than 20 publications) relating to his Ph.D. work. He is currently a Senior Lecturer (Associate Professor) of electronic and communication engineering at Wrexham Glyndwr University. He is a Chartered Engineer (CEng) with the Engineering Council.

Mr. Akinsolu is a Fellow of the Higher Education Academy (FHEA), a member of the IET (MIET), and a registered Electrical Engineer with the COREN.

Hsi-Tseng Chou (Fellow, IEEE) received the B.S. degree in electrical engineering from National Taiwan University, Taipei, Taiwan, in 1988, and the M.S. and Ph.D. degrees in electrical engineering from The Ohio State University (OSU), Columbus, OH, USA, in 1993 and 1996, respectively.

He is currently appointed as a Distinguished Professor with the Graduate Institute of Communication Engineering and Department of Electrical Engineering, National Taiwan University. He joined ElectroScience Laboratory (ESL), OSU as a Graduate Research Associate during 1991 and 1996, and as a Post-Doctoral Researcher during 1996 and 1998. He has published more than 570 journal and conference papers and holds 50 patents. His research interests include wireless communication networks, antenna design, antenna measurement, electromagnetic scattering, asymptotic high-frequency techniques, such as the uniform geometrical theory of diffraction (UTD), novel Gaussian beam techniques, and UTD type solution for periodic structures.

Dr. Chou elected as a member of URSI International Radio Science U.S. commission B and has received many awards to recognize his distinguished contributions to technological developments. Some important ones include a distinguished contribution award in promoting interacademic and industrial cooperation from the Ministry of Education, a distinguished engineering professor award from the Chinese Institute of Engineers, a distinguished electrical engineering professor award from the Chinese Institute of Electrical Engineering, and the University's Industrial Economics Contribution Award (2008), National Industrial Innovation Awards—Key Technology Elite Award (2011), and Industrial-Academia Collaboration Award (2017) all from Ministry of Economics. His work in active antenna calibration was awarded by the Ministry of Science and Technology, Taiwan, as the "Future Technology Award" in 2020. He received a distinguished research award from the Ministry of Science and Technology in 2022. He was elected in 2004 as one of the nation's ten outstanding young persons by Junior Chamber International, in 2005 a National Young Person Medal from China Youth Corps of Taiwan, and as one of the top ten rising stars in Taiwan by the Central News Agency of Taiwan. He also received outstanding branch counselor awards from IEEE including IEEE headquarter, R-10, and Taipei Section, respectively. He received the IEEE technical field undergraduate teaching award in 2014. He received the Achievement Medal in communication engineering from IET in 2021. He has served as the Chair of the IEEE AP-S Taipei Chapter and received the best chapter award in 2012 and served as the Chair of the EMC-S Taipei chapter in 2019–2021.

Yushi Liu received the B.Eng. degree in electronic information engineering from the University of Electronic Science and Technology of China, Chengdu, China, in 2017, the B.Eng. (Hons.) degree in electronics and electrical engineering from the University of Glasgow, Glasgow, U.K., in 2017, and the M.Sc. degree in electrical engineering from Tufts University, Medford, MA, USA, in 2019. He is currently pursuing the Ph.D. degree with the artificial intelligence (AI)-Driven Design Lab, University of Glasgow, Glasgow, U.K., under the supervision of Dr. Bo Liu.

From 2019 to 2020, he was appointed as a Research and Development Engineer at the Institute of Deep-sea Science and Engineering, the Chinese Academy of Sciences, Beijing, China. His research interests include machine learning, engineering optimization, and AI-driven engineering design.

Bo Liu (Senior Member, IEEE) received the B.Eng. degree from Tsinghua University, Beijing, P. R. China, in 2008, and the Ph.D. degree from the University of Leuven (KU Leuven), Leuven, Belgium, in 2012.

From 2012 to 2013, he was a Humboldt Research Fellow and was working with the Technical University of Dortmund, Dortmund, Germany. In 2013, he was appointed Lecturer at Wrexham Glyndwr University, Wrexham, U.K., where he was promoted to Reader in 2016. At present, he is a Reader at the University of Glasgow, Glasgow, U.K. He is also a senior honorary fellow at the University of Birmingham, Birmingham, U.K. He has authored or coauthored one book and more than 80 articles in renowned international journals, edited books, and conference proceedings. His research interests lie in artificial intelligence (AI)-driven design methodologies of analog/RF integrated circuits, microwave devices, MEMS, evolutionary computation, and machine learning. In terms of AI-driven antenna design, he is the inventor of the SADEA algorithm series.